# Nonlinear Finite Element Analysis of a FRP-Strengthened Reinforced Concrete Bridge

Kasidit Chansawat[1]; Solomon C. S. Yim, M.ASCE[2]; and Thomas H. Miller, M.ASCE[3]

**Abstract:** Three-dimensional nonlinear finite element (FE) models are developed to examine the structural behavior of the Horsetail Creek Bridge strengthened by fiber-reinforced polymers (FRPs). A sensitivity study is performed varying bridge geometry, precracking load, strength of concrete, and stiffness of the soil foundation to establish a FE model that best represents the actual bridge. Truck loadings are applied to the FE bridge model at different locations, as in an actual bridge test. Comparisons between FE model predictions and field data are made in terms of strains in the beams for various truck load locations. It is found that all the parameters examined can potentially influence the bridge response and are needed for selection of the optimal model which predicts the magnitudes and trends in the strains accurately. Then, using the optimal model, performance evaluation of the bridge based on scaled truck and mass-proportional loadings is conducted. Each loading type is gradually increased until failure occurs. Structural responses are compared for strengthened and unstrengthened bridge models to evaluate the FRP retrofit. The models predict a significant improvement in structural performance due to the FRP retrofit.

**DOI:** 10.1061/(ASCE)1084-0702(2006)11:1(21)

**CE Database subject headings:** Concrete, reinforced; Bridges, concrete; Finite element method; Fiber reinforced polymers.

## Introduction

Many bridges in the United States are in need of strengthening due to an increase in loading, a change in use, corrosion, etc. The Horsetail Creek (HC) Bridge in Oregon in an example of a bridge that has been classified as structurally deficient, having not been designed to carry the traffic loads common today. The HC Bridge was built in 1914. It is located in the Columbia Gorge on the Columbia River Highway, 50 km (32 mi.) east of Portland, Ore. The bridge, a reinforced concrete deck on girder bridge with spread footing foundations, is 18.28 m (60 ft) long and 7.32 m (24 ft) wide. It has three 6.10 m (20 ft) spans across the Horsetail Creek. The fiber-reinforced polymer (FRP) rehabilitation to correct the structural deficiency was completed in 1998. Fig. 1 shows the bridge elevation. The bridge was rated to have only 6% of the required shear capacity for the transverse beams and only 34% for the longitudinal beams, due to the absence of shear reinforcement. Moreover, the transverse beams had only approximately 50% of the required flexural capacity (CH2M 1997). Exposed, corroded reinforcing steel was also found during an on-site inspection. However, the overall condition of the structure was good.

The Oregon Department of Transportation (ODOT) increased the load-carrying capacity of the bridge by strengthening it with FRP materials. FRP sheets were applied to both transverse and longitudinal beams to address the deficiency in shear and flexural capacities. The transverse beams required both shear and flexural strengthening, while the longitudinal beams only needed shear strengthening. Carbon FRP (CFRP) flexural and Glass FRP (GFRP) shear laminates were attached to the bottom and sides of the transverse beams, respectively, while only GFRP laminates were attached to the sides of the longitudinal beams. In general, these FRP materials were easy to install and provided a cost-effective retrofit for the bridge.

Structural characteristics of reinforced concrete (RC) bridges strengthened with FRP composites, such as inelastic response, load distribution characteristics, and ultimate strength cannot be realistically assessed with simple procedures currently used in design and evaluation. Experimental tests are sometimes expenive and time consuming, in terms of the number of specimens and parameters for the investigation. Comprehensive analytical studies, if property conducted, can provide reliable estimates of response in lieu of experimental tests for these bridge structures. Nonlinear finite element (FE) analysis is thus used in this study.

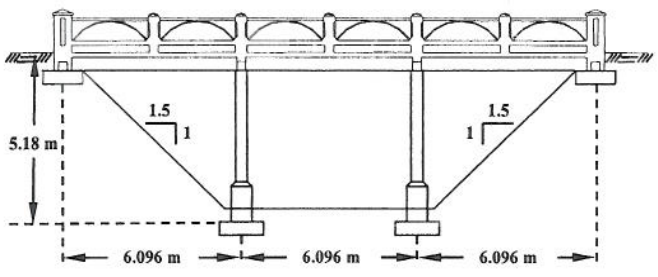


**Fig. 1.** Horsetail Creek Bridge elevation

[1]Structural Engineer, CH2M HILL, Corvallis, OR 97330.

[2]Professor, Dept. of Civil, Construction, and Environmental Engineering, Oregon State Univ., Corvallis, OR 97331.

[3]Associate Professor, Dept. of Civil, Construction, and Environmental Engineering, Oregon State Univ., Corvallis, OR 97331 (corresponding author). E-mail: thomas.miller@oregonstate.edu

Note. Discussion open until June 1, 2006. Separate discussions must be submitted for individual papers. To extend the closing date by one month, a written request must be filed with the ASCE Managing Editor. The manuscript for this paper was submitted for review and possible publication on May 28, 2003; approved on December 30, 2004. This paper is part of the ***Journal of Bridge Engineering***, Vol. 11, No. 1, January 1, 2006. ©ASCE, ISSN 1084-0702/2006/1-21–32/$25.00.

In this paper, three-dimensional finite element bridge models are developed for the HC Bridge strengthened with FRP laminates. Modeling methodology and the nonlinear analysis approach of *ANSYS version 5.7* (ANSYS 2001) are presented to calibrate the FE models to best represent the actual conditions. In situ load tests were conducted, and a sensitivity study was performed. The results from the FE bridge model are compared with the field test data in terms of strains on both the transverse and the longitudinal beams versus various truck locations. Influences of various parameters on structural behavior are discussed. Bridge performance is then evaluated using the optimal FE model. Scaled truck and mass-proportional loadings are applied to the strengthened and unstrengthened bridge models to determine the effect of the FRP retrofit on structural performance.

## Modeling Methodology and Nonlinear Analysis Approach

Nonlinear FE analysis is performed using *ANSYS*, a general-purpose finite element program. This section introduces the elements chosen from the software library and the analytical approach and assumptions used in the analysis.

### Concrete

The *SOLID65* (ANSYS 2001), three-dimensional (3D) reinforced concrete solid element, is used to represent concrete in the models. The element, using a $2\times2\times2$ set of Gaussian integration points, is defined by eight nodes having three translational degrees of freedom (DOFs) at each node. This element is capable of cracking in tension and crushing in compression, although the crushing capability of the element is not used in this study.

The most important implementation of the *SOLID65* element is the proper definition of nonlinear material properties. The responses of concrete under loading (with and without confinement due to lateral ties in the columns or FRP jackets on the beams) are characterized by distinct nonlinear behavior. Complete stress–strain curves for both unconfined and confined concrete are needed to accurately predict a whole range of bridge behavior from service loading up to failure and postfailure responses. Additionally, the descending branch is needed since a portion of the concrete compression zone is usually in this range of strains at the ultimate limit state (Wang et al. 1978). The following are the constitutive relationships used in the study for unconfined and confined concrete.

### Unconfined Concrete

In this study the constitutive models of unconfined concrete for both ascending and descending parts of the compression behavior follow Desayi and Krishnan's model (Bangash 1989) [Region *ABD* in Fig. 2(a)]:

$$\sigma = \frac{E_0\varepsilon}{1+\left(\frac{\varepsilon}{\varepsilon_0'}\right)^2} \tag{1}$$

where $\varepsilon_0'=2f_c'/E_0$ and $E_0=4{,}733\sqrt{f_c'}$ (MPa) (ACI 2002).

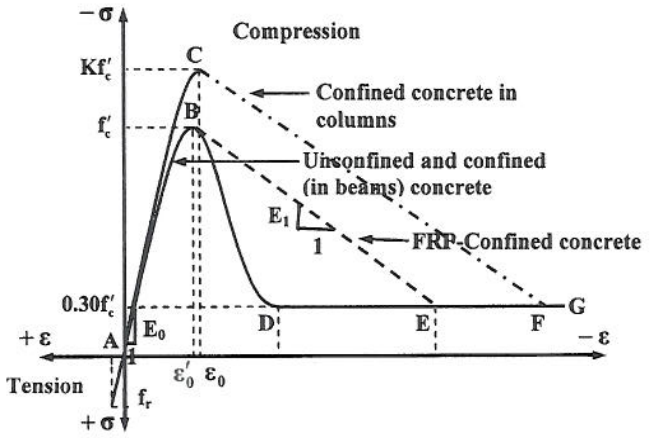


**Fig. 2.** Typical stress–strain curves of concrete

### Confined Concrete

Concrete confinement occurs when concrete under compression experiences lateral dilation due to Poisson's effect and bears against the transverse reinforcement (e.g., rectangular ties or FRP jacket), which, then, applies a confining reaction to the concrete (Kent and Park 1971). The effect of concrete confinement is taken into account in this study to avoid underestimation of the failure load (Balakrishnan et al. 1988). In this study, confined concrete can be divided into two types as follows:

#### Rectangular Tie-Confined Concrete

In general, the degree of confinement in columns with steel ties depends on the amount and spacing of steel, yield strength of steel, tie configuration, area of concrete core, concrete compressive strength, and longitudinal reinforcement. Many analytical models for the compressive stress–strain behavior of concrete confined by rectangular ties have been developed to express the increase in strength and ductility (Park et al. 1982 and Mander et al. 1988). In this study, the model proposed by Park et al. (1982) is used:

For the ascending branch (Region *AC*)

$$f_c = Kf_c'\left[\frac{2\varepsilon_c}{0.002K}-\left(\frac{\varepsilon_c}{0.002K}\right)^2\right] \tag{2}$$

where $K=1+\rho_s f_{yt}/f_c'$, and the maximum stress is assumed to be $Kf_c'$ at a strain of $\varepsilon_0=0.002K$. For the descending branch (Region *CF*):

$$f_c = Kf_c'[1-Z_m(\varepsilon_c-0.002K)]$$

where (3)

$$Z_m = \frac{0.5}{\frac{3+0.29f_c'}{145f_c'-1{,}000}+\frac{3}{4}\rho_s\sqrt{\frac{h''}{s_t}}-0.002K}$$

This is a modified form of the model of Kent and Park (1971). It improves the original Kent and Park model by taking the enhancement in the concrete strength due to confinement into account, and was especially developed for rectangular columns with rectangular steel hoops. The columns of the HC Bridge are of this configuration.

### Fiber-Reinforced Polymer-Confined Concrete

Similar to confinement in columns, concrete in beams which is restrained (due to closely spaced steel stirrups, FRP encasement, or even a localized effect of an applied concentrated load) in the direction normal to the applied stress may be considered to be confined concrete. This confinement enhances strength and ductility. A number of researchers have developed stress–strain relationships for concrete confined by steel stirrups in beams (Balakrishnan and Murray 1988 and Kemp 1998). However, the writers found no evidence of investigations of stress–strain relationships for FRP-confined concrete in flexural members. Researchers have focused on FRP confinement in columns (Teng et al. 2001). Thus, for simplicity and sufficient accuracy, as presented in Chansawat (2003), it is assumed that in beams the behavior of FRP-confined concrete is similar to that of stirrup-confined concrete. The approaches of Kent and Park (1971) and Bhatt and Kader (1998) are used. This approach assumes that the confinement has no effect on the slope of the ascending part of the stress–strain curve, and the maximum flexural stress achieved by both unconfined and confined concrete is the same and equal to $f'_c$ (Region *AB*). Based on this approach, the confinement for beams affects only the descending branch of the stress–strain curve. For the descending branch (Region *BE*), the slope of the FRP-confined concrete from Balakrishnan and Murray (1988) and Balakrishnan et al. (1988) is as follows:

$$E_1 = -0.018E_0 \tag{4}$$

For the stress–strain relationships discussed above, the cutoff point for the descending branch is assumed to be at $0.3f'_c$. Beyond this point, the concrete can still sustain stress at indefinitely large strain (Regions *DG*, *EG*, or *FG*) (Barnard 1964; Stevens et al. 1991). In the FE simulations, failure of members will occur before the concrete strain becomes excessive (Kent and Park 1971).

In the constitutive model for concrete under uniaxial tension, the material is assumed to be linearly elastic with modulus $E_0$ up to the tensile strength, $f_r$, which is calculated, based on ACI (2002)

$$f_r = 0.623\sqrt{f'_c}\ (\text{MPa}) \tag{5}$$

Typical stress–strain curves for both unconfined and confined concrete are shown in Fig. 2(a).

### Reinforcing Steel

The *LINK8*, 3D spar element, is used to represent the reinforcing steel. It is a uniaxial tension–compression element that can also include nonlinear material properties. The element has two nodes with three translational DOFs at each node.

Elastic–perfectly plastic material behavior is used for the *LINK8* element in this study.

### Fiber-Reinforced Polymer

The *SOLID46*, 3D layered structural solid element, is used to represent the FRP materials. The element has eight nodes with three translational DOFs at each node. Assuming perfect interlaminate bond, no slippage is allowed between the element layers.

The FRP laminates are considered brittle materials, and the stress–strain relationship is roughly linear up to failure. Consequently, in this study it is assumed that the stress–strain relationships for the FRP laminates are linearly elastic.

### Soil–Structure Interface Modeling

Two types of *ANSYS* elements are used for modeling the soil–structure interaction: *MATRIX27* and *SHELL143*. *MATRIX27* is an arbitrary element defined by two nodes having three translational and three rotational DOFs at each node. The element, with a stiffness specified for each DOF, serves as a multidirectional spring element representing the foundation. One *MATRIX27* element is placed at the center bottom of the column to represent the bridge footing on the supporting soil. The *SHELL143*, a four-node, plastic, small strain shell element, is used to model the "base plate" under the columns and the end abutments. This "base plate" connects the bridge structure (*SOLID65*) and the footing (*MATRIX27*) elements. The element has four nodes with six DOFs at each node. With the same DOF at each node, it is compatible with the *MATRIX27* element at the connecting node but with three more rotational DOFs than the *SOLID65* elements at the connecting surface. The stiffness of the "base plate" must be large enough to reduce the stress concentration effect at the *MATRIX27* element.

The shallow footing foundations on basalt bedrock are considered as linear-elastic springs (Jumikis 1983) having the following stiffnesses derived based on the theory of an elastic half space found in Whiteman and Richart (1967) as follows:

$$K_z = \frac{G_{\text{soil}}}{1-\nu_{\text{soil}}}\beta_z\sqrt{bd} \tag{6}$$

$$K_x = 2(1+\nu_{\text{soil}})G_{\text{soil}}\beta_x\sqrt{bd} \tag{7}$$

$$K_y = 2(1+\nu_{\text{soil}})G_{\text{soil}}\beta_y\sqrt{bd} \tag{8}$$

$$K_{mx} = \left(\frac{G_{\text{soil}}}{1-\nu_{\text{soil}}}\right)\beta_{mx}bd^2 \tag{9}$$

$$K_{my} = \left(\frac{G_{\text{soil}}}{1-\nu_{\text{soil}}}\right)\beta_{my}bd^2 \tag{10}$$

The coefficients $\beta_z$, $\beta_x$, $\beta_y$, $\beta_{mx}$, and $\beta_{my}$ can be found in Whiteman and Richart (1967). Stiffnesses are defined for the *MATRIX27* element at each DOF. Torsional stiffness (rotational stiffness about vertical axis) is not defined, as no unbalanced horizontal forces are applied in the bridge test. Soil–structure interface models, including the length and width of the footings ($b$ and $d$) are shown in Fig. 3.

A summary of the material properties used for each component in the FE bridge model is shown in Table 1.

### Nonlinear Analysis Approach

The nonlinear behavior of the structures under loading is caused not only by the transition of concrete from an uncracked to cracked state, but also by the nonlinear material properties of concrete in compression and in the steel as it yields. To obtain accurate predictions, Newton–Raphson equilibrium iteration is used to resolve for the nonlinear behavior of the bridge models using an incremental process controlled by force and displacement convergence tolerances. To avoid nonconvergence, the load must be increased gradually, and tolerances in both force and displacement criteria may have to be gradually increased along

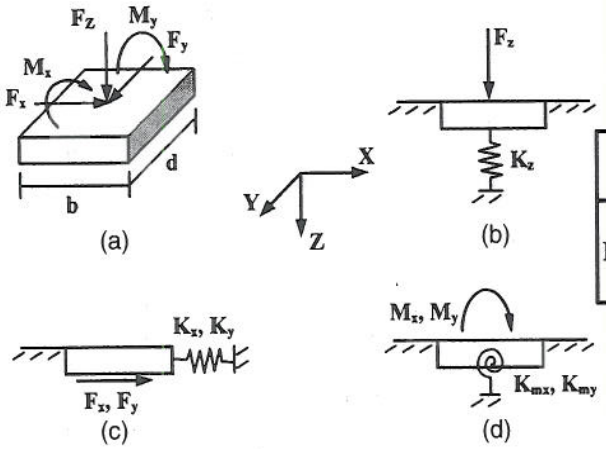


| Footing location | Footing Dimensions (m) | |
|---|---|---|
| | Length (b) | Width (d) |
| Middle columns | 1.52 | 1.52 |
| East and west columns | 1.52 | 1.37 |
| West wall | 5.79 | 0.30 |

**Fig. 3.** Soil–structure interface modeling [Hambly (1991), with permission]: (a) foundation geometry; (b) vertical stiffness; (c) horizontal stiffness; and (d) rotational stiffness

the loading history. In the sensitivity study, the maximum force and displacement convergence tolerances required were 0.5 and 1%, respectively. The maximum number of iterations per loading increment is 50.

Unlike the behavior of the HC Bridge modeled in the sensitivity study, the performance evaluation is highly nonlinear as loads approach failure. More cracking occurs, which requires many iterations in each load step. Higher convergence tolerances and computational demands are required. Force and displacement convergence criteria required were 10 and 6%, respectively, for the failure analysis of the bridge. The maximum number of iterations per loading increment was set to 50. The incremental process will stop due to solution divergence once the residual force or displacement exceeds the specified criteria. The FE solution cannot be obtained when extensive cracking causes an ill-conditioned matrix. In this case the maximum sustained load in the analysis, corresponding to the last converged load step, is used as the ultimate load prediction (Vidosa et al. 1991; Barzegar and Maddipudi 1997; Bhatt and Kader 1998).

### Analysis Assumptions

The following are the general analysis assumptions made for the HC Bridge models in this study to provide reasonable simulations for the complex behavior:

1. The bond between each element/material type are assumed perfect; that is, there is no slippage between concrete and reinforcing steel bars, between concrete and FRP laminates, and between different FRP layers. Unless the failure mode of a structure involves a bond failure, the perfect bond assumption used in the structural modeling will not cause a

**Table 1.** Material Properties

| Type of material | Material properties | | | | |
|---|---|---|---|---|---|
| | $\nu$ | E [MPa (psi)] | G [MPa (psi)] | Strength [MPa (psi)] | Thickness [mm (in.)] |
| Concrete | 0.20 | 19,700–28,900 (2.85E+0.6–4.19E+06) | — | 17.2–37.2 (2,500–5,400) | — |
| Reinforcing steel | 0.30 | 200,000 (29,000,000) | — | $f_y$=276[a] (40,000) | — |
| CFRP laminate | $\nu_{12}$=0.22 | $E_{11}$=62,100 (9,000,000) | $G_{12}$=3,270[a] (473,700) | $\sigma_{ult(ten.)}$=958[a] (139,000) | 1.1[a] (0.04) |
| | $\nu_{13}$=0.22 | $E_{22}$=4,830[a] (700,000) | $G_{13}$=3,270[a] (473,700) | Limiting strain=0.012 | |
| | $\nu_{23}$=0.30[a] | $E_{33}$=4,830[a] (700,000) | $G_{23}$=1,860[b] (270,000) | | |
| GFRP laminate | $\nu_{12}$=0.22 | $E_{11}$=20,700 (3,000,000) | $G_{12}$=1520[a] (220,000) | $\sigma_{ult(ten.)}$=600[a] (87,000) | 1.3[a] (0.05) |
| | $\nu_{13}$=0.22 | $E_{22}$=6,900[a] (1,000,000) | $G_{13}$=1,520[a] (220,000) | Limiting strain=0.012 | |
| | $\nu_{23}$=0.30[a] | $E_{33}$=6,900[a] (1,000,000) | $G_{23}$=2,650[b] (385,000) | | |
| Soil | 0.25[c] | 100–19,600[c] (1.45E+04–2.84E+06) | — | — | — |
| Base plate | 0.30 | 2.07E+11(3.00E+13) | — | — | 25.4 (1.00) |

Note: CFRP=carbon fiber-reinforced polymer and GRFP=glass fiber-reinforced polymer.

[a]Kachlakev and McCurry (2000).

[b]$G_{23}=E_2/2(1+\upsilon_{23})$.

[c]Jumikis (1983) and Hambly (1991).

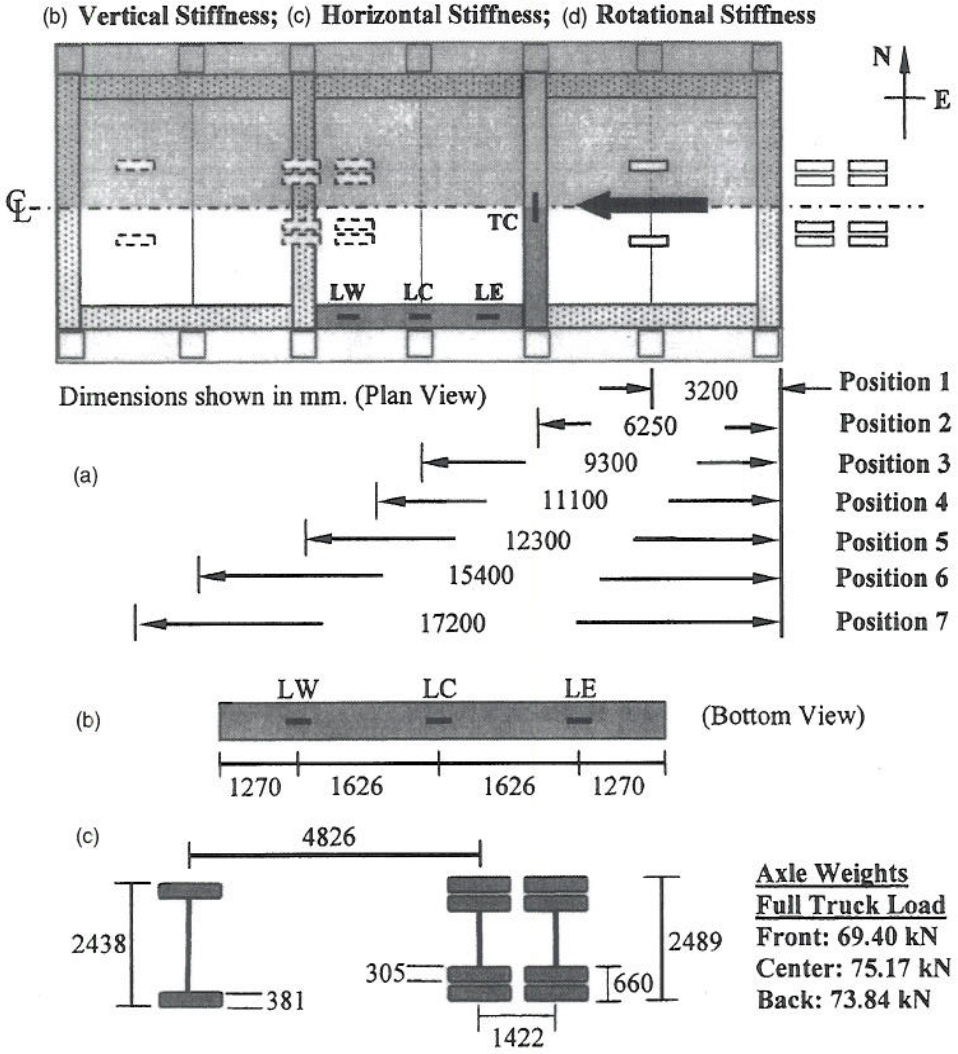


**Fig. 4.** Loading conditions: (a) locations of truck and monitored beams; (b) sensors on longitudinal beam; and (c) truck configuration

significant error in the predicted load–deflection response (Isenberg 1993).

2. A constant Poisson's ratio of 0.2 is assumed for concrete throughout the loading history.
3. For the shear transfer coefficients, β, for closed and open cracks in the *SOLID65* element, values can range from 0.0 to 1.0. A value of 0.0 refers to a smooth crack, while 1.0 refers to a rough crack. These factors are used to determine how much shear force can be transferred across open or closed cracks. For closed cracks, β is always assumed to equal 1.0. However, for an open crack, β varies from 0.05 to 0.5 (Bangash 1989). In this study, a β value of 0.2 for open cracks is used. This value is selected based on results in Chansawat (2003).
4. The concrete is assumed to be isotropic prior to cracking and orthotropic after cracking (Isenberg 1993; ANSYS 2001). The steel is assumed to be isotropic. The FRP material is assumed to be specially orthotropic, transversely isotropic. That is, the material properties in the two directions that are both perpendicular to the fiber direction are identical.
5. No failure occurs at the soil foundation.
6. Time-dependent nonlinearities such as creep, shrinkage, and temperature change are not included in this study.

## Horsetail Creek Bridge Experiment and Finite Element Modeling

### *Loading Conditions and Field Data for Sensitivity Study*

Field test data for the bridge were provided by the ODOT. The tests involved two different truck loading levels applied along the centerline of the bridge deck: empty and full truck loads. Strain data (1 microstrain precision) were collected for seven locations of the truck for both load levels. Fiber optic sensors were attached to both the concrete and FRP laminates to measure strains occurring from the truck load tests. They were located on one transverse beam and one longitudinal beam of the bridge as shown in Fig. 4. Field data were collected after FRP strengthening.

In this paper, only the full truck load level is examined. Strain measurements are taken at the midspan of a transverse beam (Point *TC*) and at three locations on a longitudinal beam (Points *LE*, *LC*, and *LW*) (*T*=transverse beam; *L*=longitudinal beam; and *E*, *C*, and *W*=east, center, and west sides, respectively). All measurements are taken at the center bottom fiber of the concrete beam section. Each sensor is 1 m long. As shown in Fig. 4(a),

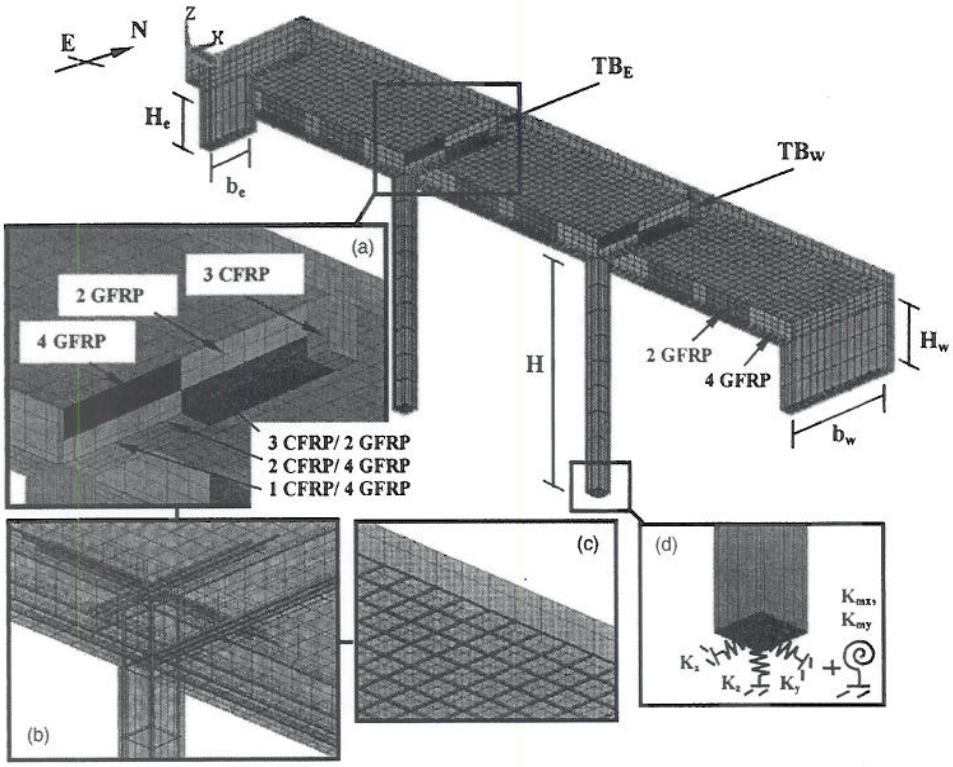


**Fig. 5.** Finite element bridge modeling: (a) typical fiber-reinforced polymer reinforcement; (b) typical steel reinforcement in beams and columns; (c) typical steel reinforcement in bridge deck; and (d) typical soil–structure interface modeling

the position of the truck is defined by the distance to the front axle from the east end of the bridge. Note that the wheel location is shown only for Positions 1 (solid rectangles) and 7 (dashed rectangles) in Fig. 4(a). The locations of the transverse and longitudinal beams with the fiber optic sensors attached are shown in Figs. 4(a and b) in the shaded area. The configuration of the truck used in the field test is shown in Fig. 4(c).

### Finite Element Modeling

The constitutive models, *ANSYS* element types, material properties, and assumptions previously discussed are used in the FE analysis. Unconfined concrete is used for the bridge deck, the cover of the columns, the curb of the bridge, and both transverse and longitudinal beams of the unstrengthened bridge for the performance evaluation. Taking advantage of symmetry, only a longitudinal half of the bridge is modeled, as shown by the lighter area (the bottom half) in Fig. 4(a). For the final model, used to best represent the actual bridge conditions after FRP retrofit, the total number of elements is 16,791: 10,504 elements for concrete (*SOLID65*), 4,954 elements for steel bars (*LINK8*), 1,168 elements for FRP (*SOLID46*), 160 *SHELL143* elements, and 5 *MATRIX27* elements. The unstrengthened bridge model lacking the *SOLID46* elements has 1,168 elements fewer. It should be noted that the thickness of the FRP laminates, which varies along the actual bridge retrofit due to different combinations of CFRP and GFRP laminates, is kept constant in the model using an equivalent thickness method. For example, if the actual laminate thickness over a certain region is reduced by half, the modulus of elasticity and shear modulus in each direction are halved in the model. The Poisson's ratios are independent of the thickness of laminate and are kept the same throughout. Fig. 5 shows the FE model of the bridge with FRP reinforcement.

## Calibration of Finite Element Models with Field Test Measurements

### Strength of In Situ Concrete

The strength of in situ concrete is an important parameter for FE models of existing RC structures. Core sample testing can be performed to examine the actual concrete strength. However, such invasive testing was not an option for this historic structure. Instead, pulse-velocity tests were conducted to provide an estimate of the strength of the in situ concrete. The range of measured concrete strength is between 25.9 MPa (3,750 psi) and 32.1 MPa (4,650 psi). To conservatively evaluate the strength of the HC Bridge before and after FRP retrofitting, 17.2 MPa (2,500 psi) compressive strength of concrete was initially assumed [Case (a) in Table 2], as per AASHTO bridge rating recommendations for all bridges built prior to 1959 (AASHTO 1994). The actual compressive strength of the concrete (and modulus of elasticity) is likely higher than this value. The sensitivity study strongly suggests that the actual concrete strength is within the range obtained from the pulse velocity measurements, and therefore higher than that recommended by AASHTO, as expected.

### Foundation Modeling

Foundation rigidity can make a large difference in the distribution of forces throughout a bridge structure. Continuous structures (e.g., the HC Bridge) can be very effective at redistributing forces, but they are also very sensitive to support conditions and foundation stiffnesses (Hambly 1991). Additionally, differential settlement of supports can induce significant bending in continuous structures. Therefore, realistic soil–structure interface

**Table 2.** Summary of Sensitivity Study

| Case | Precracking load (kN) | Material properties [$E_{soil}$ (MPa)] $f'_c$ (MPa) | Under columns | East end | West end | $E_{base\ plate}$ (GPa) | Geometrical properties $W_w$ (m) | $b_w$ (m) | $H_w$ (m) | $H$ (m) | $H_e$ (m) | $b_e$ (m) | Sum of squares |
|---|---|---|---|---|---|---|---|---|---|---|---|---|---|
| (a) No precracking load | | | | | | | | | | | | | |
| L1-1 | — | 17.24 | Fixed | Fixed | Fixed | 2.07E+08 | 0.91 | 0.00 | 0.00 | 4.88 | 0.00 | 0.00 | 1,089.0 |
| L1-2 | — | 22.06 | Fixed | Fixed | Fixed | 2.07E+04 | 0.31 | 0.00 | 0.00 | 4.88 | 0.00 | 0.00 | 1,738.3 |
| L1-3 | — | 27.58 | Fixed | Fixed | Fixed | 2.07E+08 | 0.91 | 0.00 | 0.00 | 4.88 | 0.00 | 0.00 | 2,953.7 |
| L1-4 | — | 27.58 | 19,600 | 19,600 | 19,600 | 2.07E+08 | 0.91 | 0.00 | 0.00 | 4.88 | 0.00 | 0.00 | 2,942.2 |
| L1-5 | — | 27.58 | 19,600 | 100 | 100 | 2.07E+08 | 0.91 | 0.00 | 0.00 | 4.88 | 0.00 | 0.00 | 2,537.9 |
| L2-1 | — | 17.24 | Fixed | Fixed | Fixed | 2.07E+08 | 0.91 | 2.90 | 1.52 | 5.49 | 1.22 | 1.07 | 924.9 |
| L2-2 | — | 17.24 | 100 | 100 | 100 | 2.07E+08 | 0.31 | 2.90 | 1.52 | 5.49 | 1.22 | 1.07 | 1,160.4 |
| L3 | — | 17.24 | Fixed | Fixed | Fixed | 2.07E+08 | 0.91 | 2.90 | 1.52 | 6.10 | 1.83 | 0.00 | 597.3 |
| (b) Moderate precracking load | | | | | | | | | | | | | |
| NL2-1 | 1,680 | 27.58 | 19,600 | 19,600 | 19,600 | 2.07E+08 | 0.31 | 2.90 | 1.52 | 5.49 | 1.22 | 1.07 | 4,086.5 |
| NL2-2 | 1,680 | 32.41 | 19,600 | 19,600 | 19,600 | 2.07E+08 | 0.31 | 2.90 | 1.52 | 5.49 | 1.22 | 1.07 | 3,533.5 |
| NL2-3 | 1,680 | 37.23 | 19,600 | 19,600 | 19,600 | 2.07E+08 | 0.31 | 2.90 | 1.52 | 5.49 | 1.22 | 1.07 | 1,139.6 |
| (c) Initial precracking load | | | | | | | | | | | | | |
| NL2-4 | 1,399 | 27.58 | 19,600 | 19,600 | 19,600 | 2.07E+08 | 0.31 | 2.90 | 1.52 | 5.49 | 1.22 | 1.07 | 128.7 |
| NL2-5 | 1,479 | 31.03 | 19,600 | 19,600 | 19,600 | 2.07E+08 | 0.31 | 2.90 | 1.52 | 5.49 | 1.22 | 1.07 | 214.9 |
| NL3-1 | 1,319 | 27.58 | 19,600 | 19,600 | 19,600 | 2.07E+08 | 0.31 | 2.90 | 1.52 | 6.10 | 1.83 | 0.00 | 105.9 |
| NL3-2 | 1,311 | 27.58 | 490 | 980 | 200 | 2.07E+08 | 0.31 | 2.90 | 1.52 | 6.10 | 1.83 | 0.00 | 100.1 |
| NL3-3 | 1,311 | 27.58 | 980 | 490 | 200 | 2.07E+08 | 0.31 | 2.90 | 1.52 | 6.10 | 1.83 | 0.00 | 95.9 |
| NL3-4 | 1,315 | 27.58 | 490 | 490 | 200 | 2.07E+08 | 0.31 | 2.90 | 1.52 | 6.10 | 1.83 | 0.00 | 93.6 |
| NL3-5 | 1,319 | 27.58 | 490 | 2,450 | 345 | 2.07E+08 | 0.31 | 2.90 | 1.52 | 6.10 | 1.83 | 0.00 | 95.8 |
| NL3-6 | 1,315 | 27.58 | 490 | 490 | 345 | 2.07E+08 | 0.31 | 2.90 | 1.52 | 6.10 | 1.83 | 0.00 | 96.1 |
| NL3-7 | 1,315 | 27.58 | 655 | 655 | 200 | 2.07E+08 | 0.31 | 2.90 | 1.52 | 6.10 | 1.83 | 0.00 | 89.4 |
| NL3-8 | 1,315 | 27.58 | 483 | 483 | 483 | 2.07E+08 | 0.31 | 2.90 | 1.52 | 6.10 | 1.83 | 0.00 | 97.7 |
| NL3-9 | 1,315 | 27.58 | 655 | 655 | 655 | 2.07E+08 | 0.31 | 2.90 | 1.52 | 6.10 | 1.83 | 0.00 | 92.0 |
| NL3-10 | 1,315 | 27.58 | 827 | 827 | 827 | 2.07E+08 | 0.31 | 2.90 | 1.52 | 6.10 | 1.83 | 0.00 | 90.1 |
| NL3-11 | 1,315 | 27.58 | 1,000 | 1,000 | 1,000 | 2.07E+08 | 0.31 | 2.90 | 1.52 | 6.10 | 1.83 | 0.00 | 89.5 |
| NL3-12 | 1,315 | 27.58 | 1,172 | 1,172 | 1,172 | 2.07E+08 | 0.31 | 2.90 | 1.52 | 6.10 | 1.83 | 0.00 | 89.3 |
| NL3-13 | 1,315 | 27.58 | 1,345 | 1,345 | 1,345 | 2.07E+08 | 0.31 | 2.90 | 1.52 | 6.10 | 1.83 | 0.00 | 89.4 |
| NL3-14 | 1,315 | 27.58 | 1,517 | 1,517 | 1,517 | 2.07E+08 | 0.31 | 2.90 | 1.52 | 6.10 | 1.83 | 0.00 | 89.9 |

Note: L=no precracking load (essentially linear analysis); NL=with precracking load (nonlinear analysis); and Fixed=sufficiently high $E_{soil}$ is used to provide a fixed boundary condition.

modeling is needed. $E_{soil}$ and $\nu_{soil}$ are required to determine the spring stiffnesses in the interface modeling, as previously presented. The HC Bridge is in a zone of basalt bedrock. $E_{basalt}$ can range between 20 GPa ($2.8\times10^6$ psi) 10 GPa ($16\times10^6$ psi) $\nu_{soil}$ can range between 0.14 and 0.25 (Jumikis 1983).

### Comparison Procedure

Two parameters that can significantly affect the bridge structural behavior; i.e., the in situ concrete strength and soil stiffness, are unknown. However, from the pulse velocity measurements and the geological evidence, reasonable ranges for these unknown properties are obtained. Besides these parameters, some geometrical properties of the bridge are also unknown, such as the actual depths of the footings. Existing crack patterns on the bridge were not mapped before FRP strengthening. A sensitivity study is therefore required to investigate these unknown parameters and develop a model to best simulate actual bridge conditions.

Sum of squares (SS) of differences is used as a criterion in the sensitivity study to calibrate the model. Comparison is made for the strain plots between FE predictions and field data. The SS is calculated based on the data of four strain locations (*TC*, *LE*, *LC*, and *LW*) for all seven truck locations, as expressed in the following equation:

$$SS = \sum_{i=1}^{4}\sum_{j=1}^{7}(\varepsilon_{FEM_j} - \varepsilon_{EXP_j})_i^2 \tag{11}$$

The minimum SS implies the best model, which most closely predicts the strain results from the bridge test. A summary of the sensitivity study varying parameters, including the SS for each case, is shown in Table 2. Forty-two sensitivity analyses were performed varying the concrete strength, soil stiffness for each foundation location, bridge geometry, and damage level of the bridge. As can be seen from Table 2, the bridge model with reasonable material properties and the minimum SS is model NL3-12. This model has $f'_c$=27.6 MPa and $E_{soil}$=1,171 MPa. It should be noted that only 27 of the 42 cases are illustrated.

To illustrate the effects of the moving truck on the structural behavior of the bridge, the strains are plotted versus the distances of the single front axle of the truck from the east end of the bridge. Basically, these plots are similar to "influence lines," but

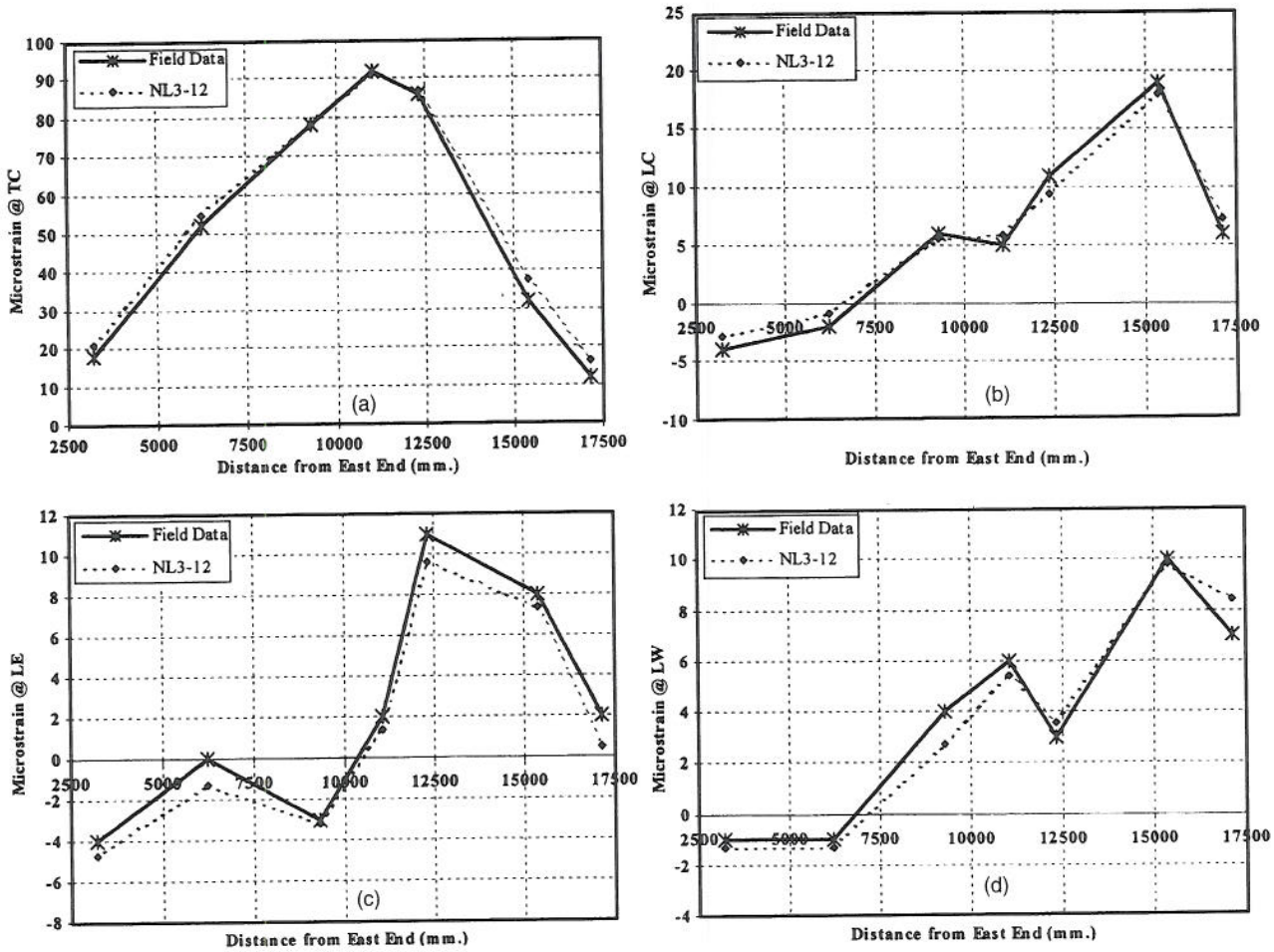


**Fig. 6.** Comparisons of strain versus truck distance between field data and finite element prediction from NL3-12 for each sensor

for a truck instead of a unit load. Comparisons of the strains between the FE analysis based on the best model (NL3-12) and the field data are shown in Figs. 6(a–d). As seen in the figures, the proposed model predicts very well both magnitudes and trends in the strains for the various truck load locations. As can be seen in Fig. 6, the peak observed strains generally occur when the rear tandem of the truck is nearest the gage considered.

### Loading Procedures

Two main loadings are applied in the analysis; i.e., a precracking loading (if performed) and truck load steps. The precracking loading is applied using a uniformly distributed load on the bridge deck and, then, the load is gradually increased until the bridge starts cracking. After the cracks are introduced to the bridge model, the load is gradually removed. Following that, the truck load is gradually applied on the bridge deck at each location for the various analyses. Self-weight of the bridge is not included because the strains from the tests did not account for the strains induced by the self-weight.

### Sensitivity Study

The sensitivity study provides useful understanding about how each parameter influences the bridge behavior (i.e., the strain versus truck load location relationship) and enables development of a model to best represent the actual conditions.

### Influence of Geometry of Horsetail Creek Bridge

The main models from Cases L1-1, L2-1, and L3 will be investigated (Table 2). The differences among these three models are the middle column height ($H$), heights of the east and west columns ($H_e$,$H_w$), and widths of the east and west walls ($b_e$,$b_w$). For Case L1-1, no east and west walls and columns are modeled, and the middle columns are shortest. For Case L2-1, all columns and walls are modeled. The model for the Case L3 model has the longest middle and east columns without the east wall. Other parameters are fixed for all models in order to examine only the influence of bridge geometry.

Comparisons of $TC$ and $LE$ strains for the various truck locations in each analysis are plotted against the field data in Figs. 7(a and b). For $TC$ [Fig. 7(a)], it can be seen that higher strains are observed for the model for Case L3 from Positions 1–4, due to the increase in longitudinal flexibility of the bridge. However, when the truck is moved to Positions 5–7, the decreasing trends in the strain for all the cases are similar, due to the remoteness of the load from the sensor. For $LE$ [Fig. 7(b)], higher strains for the various truck locations are obtained from the models with the longer middle columns. It should be noted that Model L1-1 most closely matches the field data for this sensor. The geometric changes insignificantly affect the strain responses at $LC$ and $LW$ (not shown here). When the west wall footing

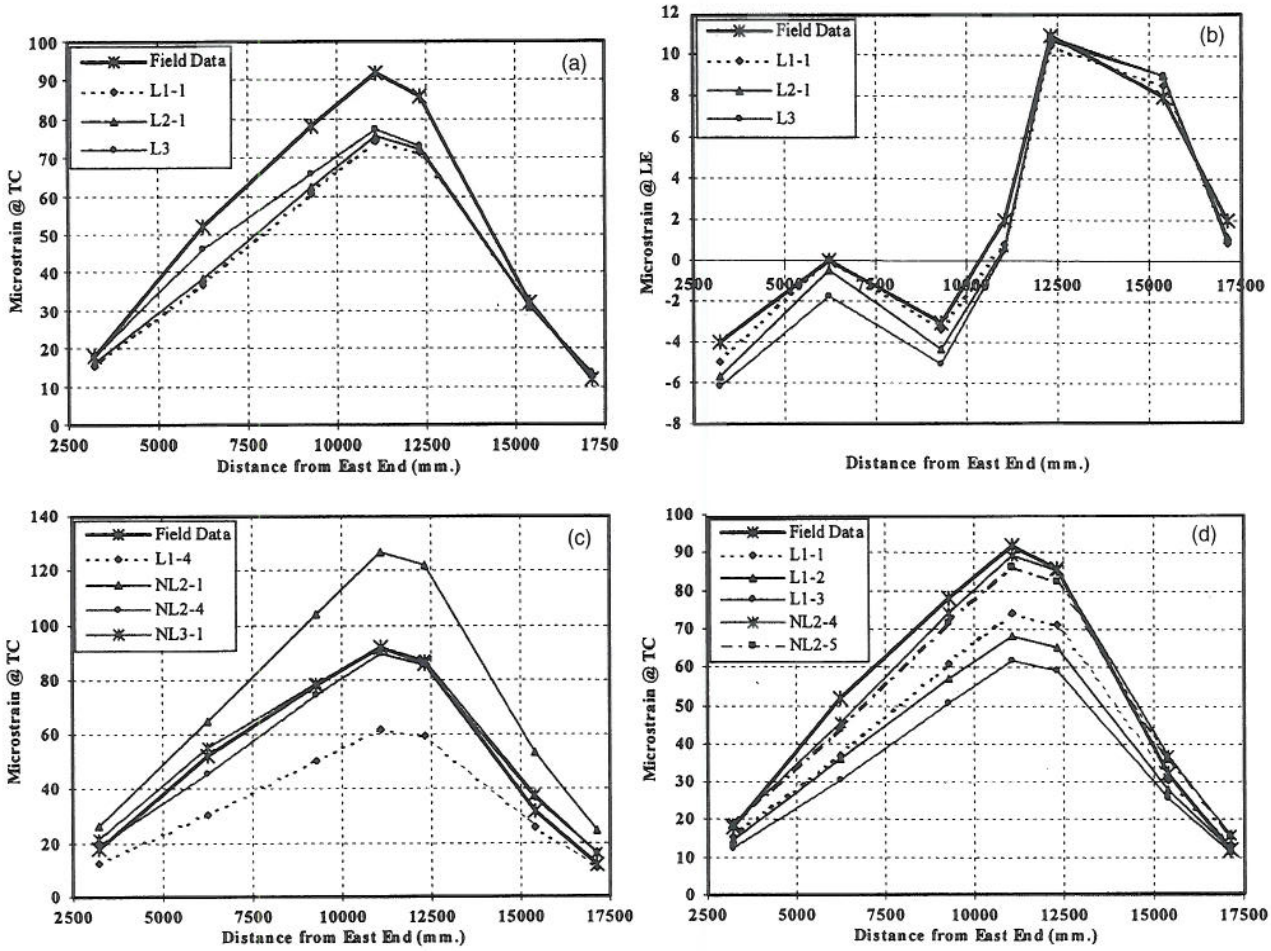


**Fig. 7.** Influences of bridge parameters: (a) and (b) bridge geometry; (c) precracking load; and (d) strength of concrete

width ($W_w$) is decreased from 0.914 to 0.305 m in the model, the trends in strains for all the cases (not shown here) show little variation.

Among these three primary models, Table 2 shows that SS for Model 3 (L3) is a minimum. The geometry of this model will be used most often when the influence of soil foundation stiffness is examined, as it most accurately predicts the strain values.

### *Influence of Precracking Load*

The bridge is cracked under a uniformly distributed precracking load before the truck load is applied, to represent existing damage to the bridge. Under the precracking load, flexural cracks are introduced around the middle span of the transverse beams. The level of damage is controlled by the magnitude of the precracking load: no precracking, initial, and moderate precracking loads. The difference between the initial and moderate precracking loads is that the initial precracking load is the lowest load to cause cracking in the bridge, while the moderate precracking load is higher and induces more cracks than the initial one. Case L1-4 as the no precracking Load Case; NL2-1 as the moderate precracking load case; and NL2-4 and NL3-1 as the initial precracking load cases are discussed (Table 2). The bridge does not crack under the applied full truck load alone (no precracking load). Therefore, the uncracked bridge structure behaves linearly. For the precracking load cases, the cracked bridge behaves nonlinearly. Structural stiffness is updated at the end of each load substep to reflect the material nonlinearities and changes in status of concrete material.

The comparison of *TC* strain results for each case is plotted in Fig. 7(c). It is obvious that the model with no precracking (L1-4) is too stiff. For a better match using the uncracked model, the strength of the concrete must be assumed to be unreasonably low [lower than 17.2 MPa (2,500 psi)]. On the other hand, if the bridge has too many cracks (see NL2-1), it becomes too flexible. In this case, the strength of the concrete must be assumed to be unrealistically high to provide a better prediction. However, when the initial precracking load (NL2-4 and NL3-1) is used, the strain predictions very closely follow the field data. They fit the field data best for NL3-1 having the same bridge geometry as Case L3. Table 2 confirms the significant improvement; i.e., the SS values are lowest after applying the initial precracking load. Therefore, the initial precracking using a uniformly distributed load is used in the model to replicate the existing cracks in the actual bridge. For sensor locations *LE*, *LC*, and *LW*, no significant variations between these models were observed.

### *Influence of Strength of In Situ Concrete*

Cases L1-1, L1-2, L1-3, NL2-4, and NL2-5 are examined to show the influence of in situ concrete strength $f'_c$. For the case with no precracking, the concrete strength varies from 17.24 to 22.06 MPa, and to 27.58 MPa for L1-1, L1-2, and L1-3, respectively. For the initial precracking load case, the concrete strength is 27.58 and 31.03 MPa for NL2-4 and NL2-5, respectively. Comparison of *TC* strain results is shown in Fig. 7(d). As concrete

strength ($f'_c$) increases, the bridge structure becomes stiffer, which in turn lowers the strains for the various truck locations in each successive case. This trend can be observed both with and without precracking loads. The results also show that when a value of $f'_c$ of 27.58 MPa is used for the initial precracking load (NL2-4), the strain predictions are closest to the field data. Moreover, the concrete strength falls within a reasonable range obtained from the pulse velocity measurements. As a result, a value of $f'_c$=27.58 MPa is assumed for the strength of the in situ concrete. Again, no significant differences are observed, due to the variation in $f'_c$, for sensor locations *LE*, *LC*, and *LW*.

### Influence of Soil Stiffness

It can be concluded from the previous discussion on the influences of bridge geometry, precracking load, and strength of concrete that varying these parameters significantly affects only the predicted *TC* strain. Additionally, the bridge geometry from Case L3, with an initial precracking load, and an $f'_c$ of 27.58 MPa should be used as a base model for the next adjustment in the sensitivity study; i.e., the influence of soil stiffness. Comparisons of strains versus the various truck locations for the study cases are made, and it can be concluded that the soil stiffness mainly affects the shape of the "influence line" for *LE*, *LC*, and *LW* strains. It also moves the curves up and down within a narrow band about the field results. Fine tuning these strain curves by varying $E_{soil}$ at the various locations is needed in order to obtain the FE model that can best represent the actual bridge conditions. Even when the lowest value for $E_{basalt}$ (19.6 GPa) is used, the response is almost the same as that of the bridge having "fixed" boundary conditions (L1-3 and L1-4), as seen from the same SS value (Table 2). The soil stiffness must be sufficiently lowered to cause the bridge model to be affected by the soil conditions. Consequently, it is assumed that there are softer soil materials than basalt between the bridge foundation and basalt bedrock and that the combined soils still behave linearly. For the extreme case, the footings are assumed to be on very stiff clay [$E_{clay}$=100 MPa from Hambly (1991)]. $E_{soil}$ will be varied between $E_{basalt}$ and $E_{clay}$.

With the base model, $E_{soil}$ is varied to fine tune the *LE*, *LC*, and *LW* strain curves from Cases NL3-1 to NL3-14. The strain results are not plotted here, as they are very close to one another. However, the SS for each case is tabulated in Table 2 to show how the changes in $E_{soil}$ improve the strain predictions. From Cases NL3-8 to NL3-14, it is assumed that the footings are on the same type of foundation, and the soil stiffness is increased by an increment of 172 MPa. Table 2 shows that the SS is lowest for Case NL3-12. As a result, the FE model from Case NL3-12 is selected to be that which can best represent the actual bridge conditions.

## Performance Evaluation

To determine the actual capacity of bridges, destructive testing has to be performed. However, the HC Bridge is a historic structure and is still operational. One practical approach is to use the analytical tool previously presented; however, one is not assured of accurately predicting the behavior of the bridge beyond service loading. The initial cracking modeled may not well represent the actual cracking (including both visible cracks and invisible microcracks) condition of such an historic bridge. However, the method of introducing initial cracks to the structure provides a stiffness as close to the actual stiffness of the bridge as possible under service loads. Two bridge models are examined; i.e., the unstrengthened and FRP-strengthened HC bridges. The strengthened bridge model is the optimal model obtained from the sensitivity study (NL3-12). The unstrengthened bridge model lacks the FRP elements (*SOLID46*) on the beams.

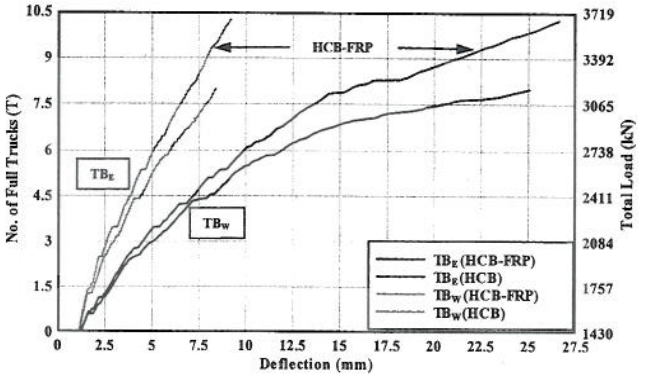


**Fig. 8.** Scaled truck load/total load–deflection relationships of transverse beams

### Performance Evaluation Based on Scaled Truck Loads

Both models are subjected to increments of the full truck load at Position 4 (Fig. 4) and are gradually loaded to failure from the virgin state (without cracks). This truck location is selected, as it induces the maximum strain in the east transverse beam. The bridge self-weight is included in the loading. The locations of the deflections of interest are at $TB_E$ and $TB_W$, as shown in Fig. 5.

From Fig. 8, the maximum scaled truck loads that can be applied to the unstrengthened and FRP-strengthened bridges are 8*T* (1*T*=1 full truck [see Fig. 4(c)] =218 kN, which is approximately equivalent to an AASHTO H16.25 truck) and 10.3*T*, respectively. The truck-carrying capacity is increased by 28% after FRP retrofit. The deflection of the strengthened beams is less than that of the unstrengthened beams at the same load level. For example, to cause $TB_E$ to deflect to a standard limit of span length (6 m)/800, it takes about 4.4*T* on the unstrengthened bridge, while 5.2*T* on the strengthened bridge. Both bridges start cracking in the transverse beams, and then cracks propagate through the deck from the bottom layer. However, a narrower band of cracks and fewer cracks can be observed in the strengthened bridge at the same load level. Fig. 9 shows a delay in tension steel yielding in the strengthened beam and the bridge deck. Fewer steel bars yield in the strengthened model at the same load level. Steel yielding in the shear zone dominates for the unstrengthened beam, while that in the flexure zone dominates for the strengthened beam. Note that the maximum strain in the CFRP at failure (4,300 microstrain) is less than the limiting strain of the CFRP in Table 1. The crack pattern and yielding in tension steel of the transverse beam from both bridge models resemble those of the full-scale unstrengthened and flexure/shear-strengthened beams which replicate the bridge beam before and after FRP retrofit (Chansawat 2003). Therefore, a shear failure is expected in $TB_E$ of the unstrengthened bridge, while a flexural failure is expected in $TB_E$ for the strengthened bridge.

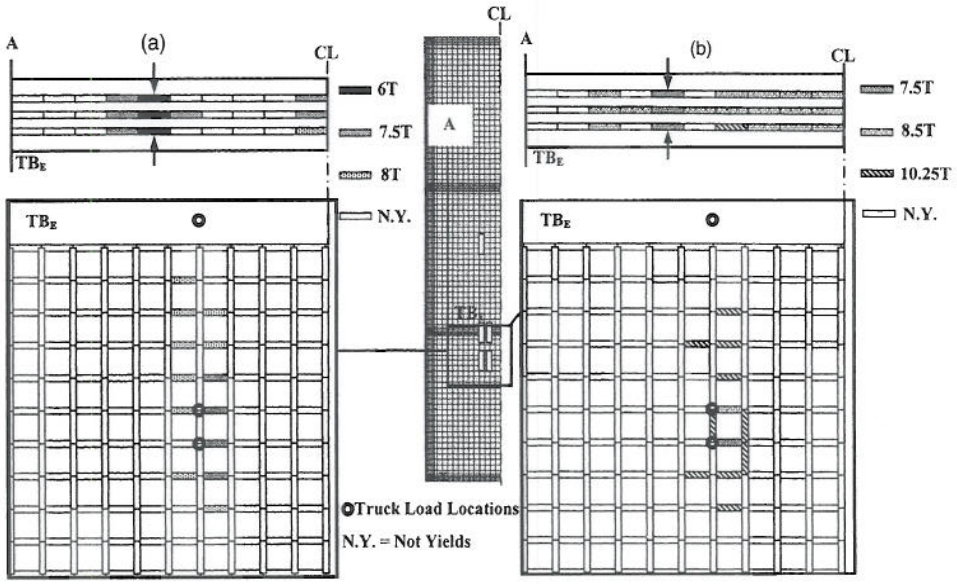


**Fig. 9.** Yielding in reinforcing steel: (a) unstrengthened bridge and (b) fiber-reinforced polymer-strengthened bridge

### *Performance Evaluation Based on Scaled Gravity Load*

As a measure of retrofit effectiveness, the two bridge models are subjected to downward, mass-proportional (gravity) loading of increasing amplitude up to failure from the virgin state. It is found that the structural behaviors of the HC Bridge before and after FRP strengthening under scaled gravity load are very similar to those under scaled truck loads. The capacity of the FRP-strengthened bridge is increased by 37% (Chansawat 2003).

## Conclusions

A sensitivity study on the influences of bridge geometry, precracking load (damage level), and strength of concrete is performed. Comparisons of the strain results between *ANSYS* predictions and the experimental data show that the proposed FE model (from Case NL3-12) is a realistic representation for the HC Bridge in terms of the number of elements, structural details, reasonable concrete and soil properties, and predicted structural response.

The bridge model must be precracked with an initial load before the service truck load is applied to take into consideration the existing damage in the actual bridge. The actual concrete strength is much higher than the value suggested by AASHTO, and is estimated using pulse-velocity measurements, verified by the sensitivity study. The estimated concrete strength from this study is 27.6 MPa (compared with the AASHTO recommended $f'_c$ of 17.3 MPa) and is within the $f'_c$ range of 25.9–32.1 MPa obtained from the pulse-velocity measurements. Soil–structure interaction modeling is important to fine tune the FE model. This is done by replacing the foundation with translational and rotational spring elements. The sensitivity study indicates that varying the soil stiffness mainly affects the predicted strains on the monitored longitudinal beam. Besides inspection of the strain plots for FE predictions and field data, the SS of the strains is used as a tool to objectively select the most representative FE model from a large number of study cases.

The bridge under the failure loads shows improvements gained from FRP strengthening. The capacities of the HC Bridge after FRP strengthening, based on scaled truck and mass-proportional loadings, are increased by 28 and 37%, respectively. Yielding of the reinforcement and crack propagation is delayed in the FRP-strengthened bridge. The failure mode of the bridge is shifted from shear failure in the transverse beams to flexural failure through the FRP strengthening. One of the limitations that should be noted is that the FE results predict failures that do not involve epoxy bond and FRP delamination. This and other failure modes need to be investigated and included in future research. Analyses starting from a precracked (rather than uncracked) state should also be performed.

## Acknowledgments

This project was supported by the Oregon Department of Transportation (ODOT), Salem, Ore., and the Department of Civil, Construction, and Environmental Engineering, Oregon State University, Corvallis, Ore. The writers wish to thank the reviewers for their valuable suggestions and comments.

## Notation

*The following symbols are used in this paper:*

$b$ = length of footing;
$b_e$ = east wall width;
$b_w$ = west wall width;
$d$ = width of footing;
$E_{\text{basalt}}, E_{\text{clay}}$ = moduli of elasticity of basalt and clay;
$E_{\text{base plate}}$ = modulus of elasticity of base plate;
$E_{\text{soil}}$ = modulus of elasticity of soil;
$E_0$ = initial modulus of elasticity of concrete in beams;
$E_1$ = slope of descending branch of fiber-reinforced polymer-confined concrete;

$E_{11}, E_{22}, E_{33}$ = moduli of elasticity of fiber-reinforced polymer in fiber direction and in axes perpendicular to fiber direction;
$F_z, F_x, F_y$ = unit vertical and horizontal forces in $x$ and $y$ directions;
$f_c$ = compressive stress in confined concrete in columns;
$f'_c$ = uniaxial compressive strength of concrete;
$f_r$ = uniaxial tensile strength (modulus of rupture) of concrete;
$f_y$ = yield strength in reinforcing steel bars;
$f_{yt}$ = yield strength of steel ties;
$G$ = shear modulus of fiber-reinforced polymer;
$G_s$ = shear modulus of soil;
$G_{12}, G_{13}, G_{23}$ = shear moduli of fiber-reinforced polymer in 1-2, 1-3, and 2-3 planes; 1-2 and 1-3 planes are planes perpendicular to fiber direction;
$H$ = middle column height;
$H_e$ = east end column height;
$H_w$ = west end column height;
$h''$ = width of concrete core measured to outside of peripheral tie;
$K$ = modification factor for confined concrete strength;
$K_{mx}, K_{my}$ = rotational spring stiffnesses about $x$ and $y$ axes;
$K_z, K_x, K_y$ = vertical and horizontal ($x$ and $y$ directions) spring stiffnesses;
$M_x, M_y$ = unit moments about $x$ or $y$ axes;
SS = sum of squares of differences;
$S_t$ = center-to-center spacing of ties;
$W_w$ = west wall footing width;
$Z_m$ = modification factor of confined concrete strength in descending branch;
$\beta$ = shear transfer coefficient;
$\beta_{mx}, \beta_{my}$ = rotational stiffness coefficients about $x$ and $y$ axes;
$\beta_z, \beta_x, \beta_y$ = vertical and horizontal ($x$ and $y$ directions) stiffness coefficients;
$\varepsilon$ = compressive strain in concrete;
$\varepsilon_c$ = compressive strain in confined concrete in columns;
$\varepsilon_{FEM}, \varepsilon_{EXP}$ = analytical and experimental strains;
$\varepsilon_y$ = yield strain in reinforcing steel bars;
$\varepsilon_0$ = compressive strain at ultimate confined compressive stress in concrete in columns;
$\varepsilon'_0$ = compressive strain at ultimate unconfined and confined compressive stress in concrete in beams;
$\nu$ = Poisson's ratio;
$\nu_{soil}$ = Poisson's ratio of soil;
$\nu_{12}, \nu_{13}, \nu_{23}$ = Poisson's ratios in 1-2, 1-3, and 2-3 planes; 1-2 and 1-3 planes are planes perpendicular to fiber direction;
$\rho_s$ = ratio of volume of rectangular steel ties to volume of concrete core measured to outside of peripheral tie;
$\sigma$ = compressive stress in concrete; and
$\sigma_{ult(ten.)}$ = ultimate tensile strength of fiber-reinforced polymer in fiber direction.

## References


American Association of State and Highway Transportation Officials (AASHTO). (1994). *Manual for condition evaluation of bridges*, AASHTO Subcommittee on Bridges and Structures, Washington D.C.

American Concrete Institute (ACI). (2002). "Building code requirements for structural concrete." *ACI 318-02*. ACI Committee 318, Farmington Hills, Mich.

*ANSYS Revision 5.7*. (2001). Swanson Analysis System, Inc., Houston.

Balakrishnan, S., Elwi, A. E., and Murray, D. W. (1988). "Effect of modeling on NLFE analysis of concrete structures." *J. Struct. Eng.*, 114(7), 1467–1487.

Balakrishnan, S., and Murray, D. W. (1988). "Concrete constitutive model for NLFE analysis of structures." *J. Struct. Eng.*, 114(7), 1449–1466.

Bangash, M. Y. H. (1989). *Concrete and concrete structures: Numerical modeling and applications*, Elsevier Science, Essex, U.K.

Barnard, P. R. (1964). "Researches into the complete stress–strain curve for concrete." *Mag. Concrete Res.*, 16(49), 203–210.

Barzegar, F., and Maddipudi, S. (1997). "Three-dimensional modeling of concrete structures. II: Reinforced concrete." *J. Struct. Eng.*, 123(10), 1347–1356.

Bhatt, P., and Kader, M. A. (1998). "Prediction of shear strength of reinforced concrete beams by nonlinear finite element analysis." *Comput. Struct.*, 68, 139–155.

Chansawat, K. (2003). "Nonlinear finite element analysis of reinforced concrete structures strengthened with FRP laminates." PhD dissertation, Oregon State Univ., Corvallis, Ore.

CH2M Hill Consulting Engineers and TAMS Consultants. (1997). "Evaluation and resolution of under capacity state bridges: Bridge No. 04543, Horsetail Creek Bridge." CH2M HILL, Inc., Corvallis, Ore.

Hambly, H. C. (1991). *Bridge deck behavior*, 2nd Ed., Clays Ltd., St Ives Plc., U.K.

Isenberg, J. (1993). *Finite element analysis of reinforced concrete structures II*, ASCE, New York.

Jumikis, A. R. (1983). *Rock mechanics*, Gulf, Houston.

Kachlakev, D. I., and McCurry, D., Jr. (2000). "Testing of full-size reinforced concrete beams strengthened with FRP composites: Experimental results and design methods verification." *SPR316*, Federal Highway Administration, United States Department of Transportation, and Oregon Department of Transportation, Salem, Ore.

Kemp, A. R. (1998). "The achievement of ductility in reinforced concrete beams." *Mag. Concrete Res.*, 50(2), 123–132.

Kent, D. C., and Park, R. (1971). "Flexural members with confined concrete." *J. Struct. Div. ASCE*, 97(7), 1969–1990.

Mander, J. B., Priestley, M. J. N., and Park, R. (1988). "Theoretical stress–strain model for confined concrete." *J. Struct. Eng.*, 114(8), 1804–1826.

Park, R., Priestley, M. J. N., and Gill, W. D. (1982). "Ductility of square-confined concrete columns." *J. Struct. Div. ASCE*, 108(4), 929–950.

Stevens, N. J., Uzumeri, S. M., Collins, M. P., and Will, T. G. (1991). "Constitutive model for reinforced concrete finite element analysis." *ACI Struct. J.*, 88(1), 49–59.

Teng, J. G., Chen, J. F., Smith, S. T., and Lam, L. (2001). *FRP strengthened RC structures*, Wiley, West Sussex, U.K.

Vidosa, F. G., Kotsovos, M. D., and Pavlovic', M. N. (1991). "Nonlinear finite element analysis of concrete structures: Performance of a fully three-dimensional brittle model." *Comput. Struct.*, 40(5), 1287–1306.

Wang, P. T., Shah, S. P., and Naaman, A. E. (1978). "Stress–strain curves of normal and lightweight concrete in compression." *J. Am. Concr. Inst.*, 75(11), 603–611.

Whiteman, R. V., and Richart, F. E. (1967). "Design procedures for dynamically loaded foundations." *J. Soil Mech. Found. Div.*, 93(6), 169–193.